Advanced Sodium Ion Battery Anode Constructed *via* Chemical Bonding between Phosphorus, Carbon Nanotube, and Cross-Linked Polymer Binder

Jiangxuan Song,[†] Zhaoxin Yu,[†] Mikhail L. Gordin,[†] Xiaolin Li,[‡] Huisheng Peng,[§] and Donghai Wang*[,†]

[†]Department of Mechanical and Nuclear Engineering, The Pennsylvania State University, University Park, Pennsylvania 16802, United States, [‡]Department of Stationary Energy Storage, Pacific Northwest National Laboratory, Richland, Washington 99354, United States, and [§]State Key Laboratory of Molecular Engineering of Polymers, Department of Macromolecular Science, and Laboratory of Advanced Materials, Fudan University, Shanghai 200438, China

ABSTRACT Maintaining structural stability is a great challenge for high-capacity conversion electrodes with large volume change but is necessary for the development of high-energy-density, long-cycling batteries. Here, we report a stable phosphorus anode for sodium ion batteries by the synergistic use of chemically bonded phosphorus—carbon nanotube (P—CNT) hybrid and cross-linked polymer binder. The P—CNT hybrid was synthesized through ball-milling of red phosphorus and carboxylic group functionalized carbon nanotubes. The P—O—C bonds formed in this process help maintain contact between phosphorus and CNTs, leading to a durable hybrid. In addition, cross-linked carboxymethyl cellulose—citric acid binder was used to form a robust electrode. As a result, this anode delivers a stable cycling capacity of 1586.2 mAh/g after 100 cycles, along with high initial Coulombic efficiency of 84.7% and subsequent cycling efficiency of ~99%. The unique electrode framework through chemical bonding strategy reported here is potentially inspirable for other electrode materials with large volume change in use.

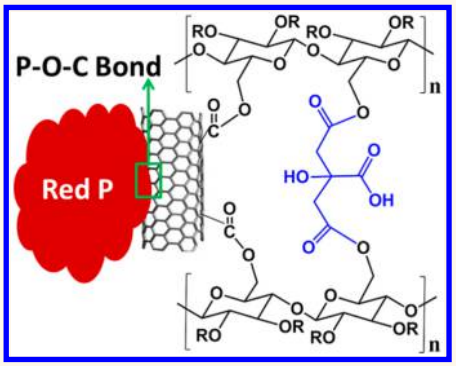

KEYWORDS: sodium ion battery · phosphorus · carbon nanotube · chemical bonding · cross-linked binder

The rapid adoption of electrical vehicles and intermittent energy sources such as solar and wind power requires reliable, low-cost, and efficient electric energy storage systems. Lithium ion batteries (LIBs) have achieved great success in the past two decades due to their high energy density and are being pursued for these growing applications.[1−14] However, due to the limited supply of lithium precursor and its uneven global distribution, the cost of LIBs may increase severely in the foreseeable future.[15−20] Therefore, it is essential to develop new low cost and sustainable energy conversion and storage technology. In this respect, room-temperature sodium ion batteries (SIBs) are attractive for energy storage due to the abundance and low price of sodium resources.[21−25] Critical obstacles still exist in the commercialization of SIBs, with the lack of suitable anode materials being one of the greatest, since commercial graphite anodes in LIBs hardly accommodate sodium ions due to size mismatch between sodium ions and the graphite lattice and thermodynamic instability of the Na—graphite system.[26−30] Conversion material can usually offer a higher capacity than that of graphite, making them promising candidates. Unfortunately, crystalline silicon, which has been widely studied in lithium ion batteries, is inactive to sodium insertion at room temperature.[31]

Recently, phosphorus has been identified as a promising anode for SIBs due to its high theoretical capacity of 2595 mAh g^{-1}, the highest among existing SIB anodes.[32−36] In addition, its low price makes it attractive as an active material for large-scale batteries. Despite these advantages, the large volume change of phosphorus upon sodiation/desodiation (>300%) makes achieving high practical capacity with long cycle life difficult. Similar to silicon in LIBs, this volume change is expected to cause poor electrical contact between phosphorus particles and the conducting matrix, pulverization of phosphorus particles, delamination of the

* Address correspondence to dwang@psu.edu.

Received for review July 19, 2015 and accepted October 25, 2015.

Published online October 25, 2015
10.1021/acsnano.5b04474

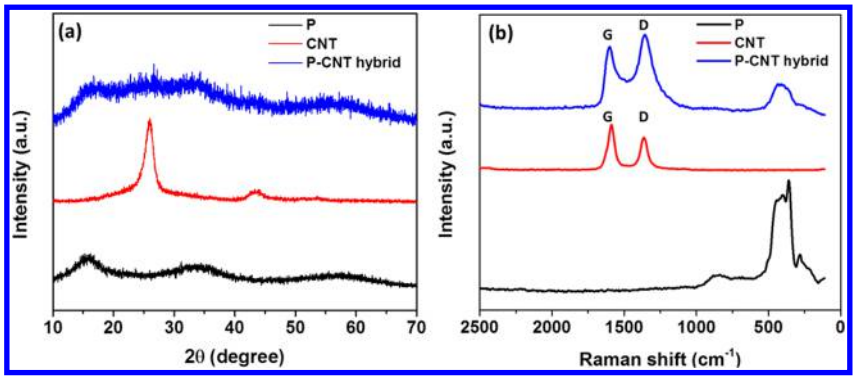

Figure 1. (a) XRD patterns of red phosphorus (P), carbon nanotube (CNT), and ball-milled P−CNT hybrid. (b) Raman spectra of ball-milled red phosphorus (P), carbon nanotube (CNT), and P−CNT hybrid.

electrode, and growth of an unstable solid−electrolyte interphase (SEI). Consequently, phosphorus anodes commonly show fast capacity fading, low Coulombic efficiency, and electrode deterioration upon cycling.[32,33] To address these issues, the phosphorus−carbon composites, including phosphorus−carbon black and phosphorus−raw carbon nanotube, were developed as sodium ion battery anodes *via* ball-milling or hand-milling methods. The mechanical force enables relatively good distribution of phosphorus particles in the carbon matrix, thus enhancing the conductivity of the composites.[32−35] Although this research shows some encouraging results for high reversible capacity, relatively fast capacity fading (<60% retention after 100 cycles) and limited cycle life (30 cycles) were shown.[32−34] The unsatisfactory electrochemical performances may due to the poor physical interaction between phosphorus particles and carbon matrix, which cannot endure the large volume changes of phosphorus electrode upon cycling.[37,38] Very recently, Wang *et al*. developed a red phosphorus/carbon nanotube composite anode *via* a vaporization−condensation approach.[36] The mechanically strong CNT network can enhance the conductivity of the composite, and thus, this composite anode delivered a capacity of ~550 mAh/$g_{composite}$ upon extended 200 cycles at 500 mA/g. This indicates that the maintenance of electrical conductivity of phosphorus and structure integrity of the electrode play a critical role in the electrochemical performance of phosphorus-based anodes. In view of these promising works, the strong interaction beyond physical interaction between phosphorus particle and conductive matrix used in the aforementioned literature is desirable for high-performance phosphorus-based electrodes.

Recent work found that chemical bonding between carbon and phosphorus can help maintain the close contact of phosphorus and carbon during cycling, thereby improving the cycling life.[37,38] Despite the important role of chemical bonding in maintaining electrical contact, it is insufficient for maintaining the structure of the whole electrode, composed of many particles and multiple components (active materials, conductive additive, binder, and current collector) in terms of the huge volume change upon cycling. In addition, the reported layer-structured graphene sheets exhibit a large irreversible capacity loss, limiting the initial Coulombic efficiency of the phosphorus-based anode.[38] Thus, novel phosphorus−carbon composite electrode materials with robust and durable binding of different electrode components is desirable for developing long cycle life, high energy density sodium ion batteries.

Here, we report a stable phosphorus anode for sodium ion batteries by integrating red phosphorus (P), carbon nanotubes (CNTs), and polymer binder through multicomponent chemical bonding. To this end, red phosphorus was chemically bonded to the CNTs *via* P−O−C bonds formed during ball-milling the mixture of phosphorus and carboxyl-groups-functionalized CNT. These P−CNT hybrid particles were further bonded together with a cross-linked polymer (sodium carboxylmethyl cellulose−citric acid, c-NaCMC−CA) to form a robust electrode. The −OH group of NaCMC is not only cross-linked with citric acid but also chemically bonded with carboxyl group functionalized CNT *via* esterification. Thanks to close contact and its durable structure due to chemical bonding, the P−CNT composite anode with cross-linked polymer binder delivered a specific capacity of 2134 mAh g^{-1} with a good cycling stability (~91% capacity retention relative to the second-cycle capacity) for over 100 cycles.

RESULTS AND DISCUSSION

The P−CNT hybrid was prepared by a facile ball-milling approach. Briefly, commercial red phosphorus and carboxyl group functionlized CNTs (7:3, weight ratio) were placed in a stainless steel ball-milling jar under argon atmosphere, followed by ball-milling, yielding P−CNT hybrid (see the Experimental Section for details). Figure 1a shows the diffraction pattern of ball-milled P−CNT hybrid; only a few very broad peaks are observed, indicating its amorphous structure.

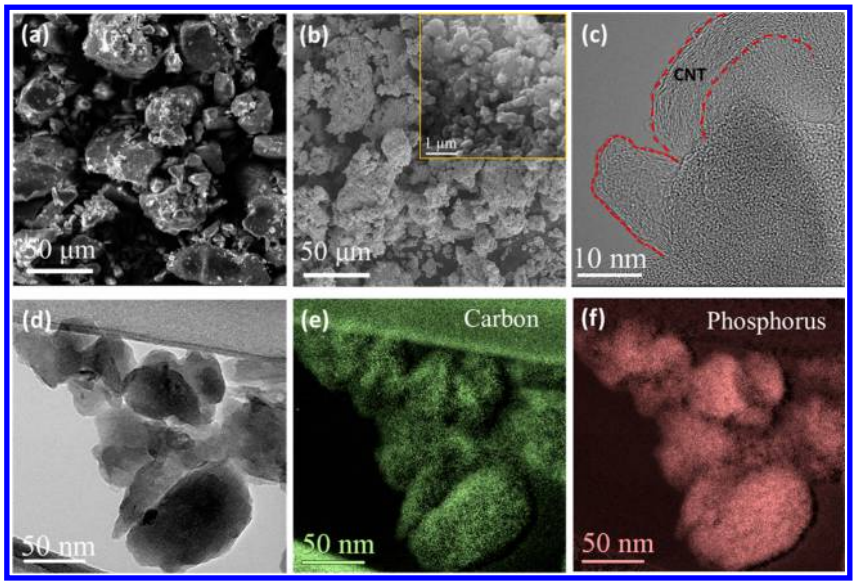

Figure 2. (a) SEM image of pristine phosphorus particles. (b) Low and high (inset) magnification SEM images of the P−CNT hybrid. (c) High magnification TEM image of P−CNT hybrid. (d) Medium magnification TEM image and (e and f) corresponding energy filtered element mapping of the P−CNT hybrid: (e) carbon and (f) phosphorus.

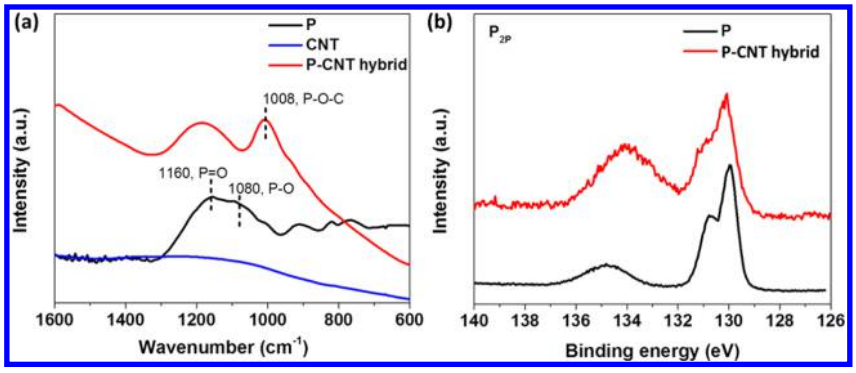

Figure 3. (a) FT-IR spectra of P, CN,T and P−CNT hybrid. (b) P 2p XPS spectra of P and P−CNT hybrid.

This is further demonstrated by the apperance of a diffuse ring in the selected area electron diffraction pattern of the P−CNT hybrid (Figure S1). The disappearance of graphitic reflection peaks (25.9° and 42.7°) seen in pristine CNTs is most likely due to shortening and deformation of the CNTs under mechanical impact and shear force during ball-milling.[39] This is further confirmed by the increased intensity of the D band of the C−C bond in the Raman spectra of the P−CNT hybrid as shown in Figure 1b. The P−CNT hybrid particles (Figure 2b) were found to be much smaller than the bulk phosphorus particles (Figure 2a), ranging from submicron to a few microns in size. The high-magnification transmission electron microscopy (TEM) image (Figure 2c) revealed that the CNTs were closely attached to the surface of red phosphorus particles. To further clarify the structure of P−CNT hybrid, elemental mapping was conducted using energy-filtered TEM (EF-TEM) as shown in Figure 2d−f. The carbon and phosphorus can be found all over the samples, indicating the uniform mixing of phosphorus and CNT in the hybrid. The primary domains of phosphorus in the hybrid as indicated by the phosphorus element mapping (Figure 2f) are in the range of 10−200 nm. The uniform distribution of phosphorus and carbon and their intimate contact allow for fast electron transfer.[40]

Mechanical force has previously been shown to induce formation of covalent bond in other phosphorus/carbon composite materials.[37,38] Fourier transform infrared spectroscopy (FT-IR) and X-ray photoelectron spectroscopy (XPS) were conducted to investigate the interaction between amorphous P and CNTs in the P−CNT hybrid. The appearance of P═O (1160 cm^{-1}) and P−O (1080 cm^{-1}) characteristic peaks in the FT-IR spectra (Figure 3a) of phosphorus indicated the existence of a thin layer of phosphorus-based oxides due to oxidation when exposed to air.[41,42] Noticeably, a new peak centered at 1008 cm^{-1} appears in the FT-IR spectra of the P−CNT hybrid. This indicates the formation of P−O−C bonds during ball-milling.[38] Three peaks centered at 129.8, 130.7 (shoulder peak), and 134.8 eV were observed in the P_{2P} XPS spectrum of the phosphorus (Figure 3b). The peaks at 129.8 and 130.7 eV can be attributed to the $P_{2p3/2}$ and $P_{2p1/2}$, respectively.[43,44] The

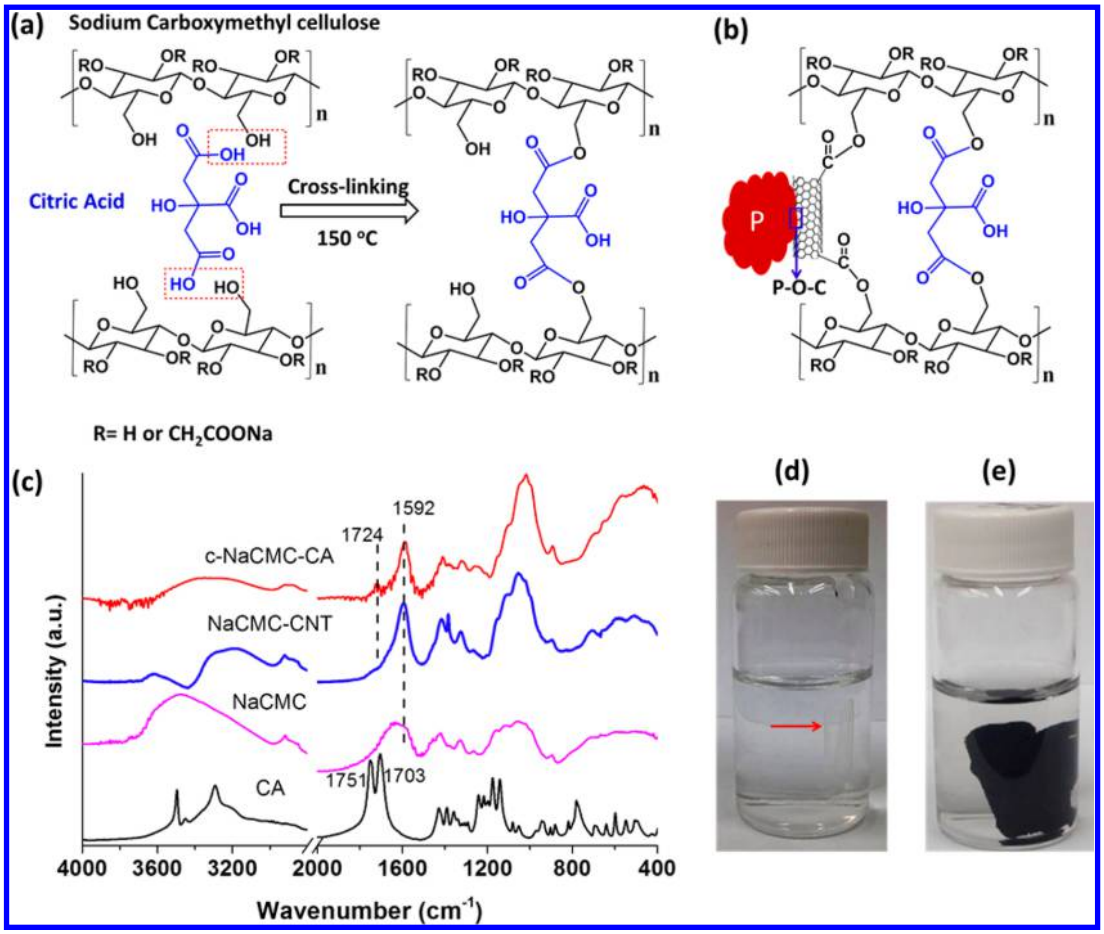

Figure 4. (a) Cross-linked polymer binder formed by thermally induced condensation of carboxymethyl cellulose and citric acid (c-NaCMC−CA). (b) Interaction between P−CNT hybrid and c-NaCMC−CA binder; (c) FT-IR spectra of citric acid (CA), NaCMC, c-NaCMC−CA, and NaCMC−CNT. Photo images of (d) c-NaCMC−CA film and (e) NaCMC−CNT composite film after 2 days' storage in deionized water at room temperature.

relatively broad higher binding energy peak at 134.8 eV arises from phosphates.[42] In contrast, in the P_{2p} spectrum of the P−CNT hybrid, an additional peak is observed at medium binding energy (~132−133 eV). This may arise from the P−O−C or P−C bonding; however, the characteristic peak (~700 cm^{-1}) of P−C bond does not appear in the Raman spectra (Figure 1), suggesting that the binding energy shift of P_{2p} in the P−CNT hybrid is due to the formation of a P−O−C bond.[37,38] This result is also consistent with the FT-IR observations. This chemical bonding enables the CNT to bind strongly with the phosphorus particles and thereby helps prevent the loss of electrical contact between phosphorus particles and the conducting carbon network during electrochemical cycling, increasing the durability of the structure.

Polymer binder, one of the major components in an electrode, plays an important role in cell electrochemical performance, especially for the cycle life and irreversible capacity losses.[2,11,45] As mentioned previously, phosphorus can have a large volume change of over 300% during charge and discharge, making it difficult to maintain the electrode structure. To integrate P−CNT hybrids particles into electrodes with good structural stability, a novel polymer binder with a cross-linked network structure was exploited. This was accomplished by utilizing aqueous NaCMC as a polymer matrix and citric acid as a cross-linker. *In situ* formation of the network was conducted by drying electrodes composed of P−CNT hybrid, conducting additives, NaCMC, and CA at 150 °C (see details in the Experimental Section). The chemical bonding between these electrode components was schematically shown in Figure 4a,b. To elucidate the interactions among NaCMC, CA, and the P−CNT hybrid, NaCMC−CNT composite and c-NaCMC−CA film were prepared following the same protocol and characterized by FT-IR spectroscopy, as shown in Figure 4c. When citric acid was introduced as a cross-linker to NaCMC, the new peaks at 1724 and 1592 cm^{-1} were observed, which are attributed to carbonyl (−C═O) and carboxylate (O═C−O) in ester groups, respectively. These changes indicate that NaCMC was cross-linked by CA through the esterification reaction between −OH of NaCMC and −COOH of CA.[46,47] The NaCMC can be easily dissolved in water and is a well-known aqueous

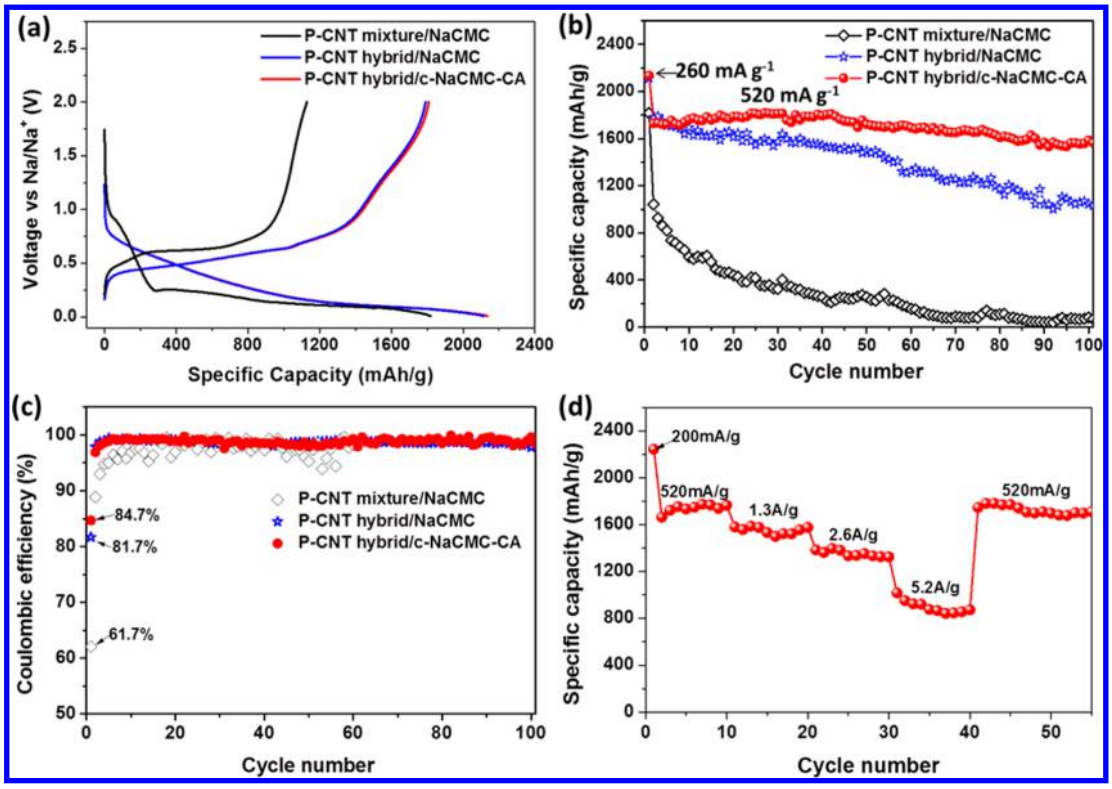

Figure 5. (a) Initial charge−discharge voltage profiles of P−CNT mixture with NaCMC binder (P−CNT mixture/NaCMC), P−CNT hybrid with NaCMC binder (P−CNT hybrid/NaCMC), and P−CNT hybrid with cross-linkd NaCMC-CA binder (P−CNT hybrid/c-NaCMC−CA). (b) Cycling stability and (c) Coulombic efficiency of the P−CNT mixture/NaCMC, P−CNT hybrid/NaCMC, and P−CNT hybrid/c-NaCMC−CA electrode at a current density of 260 mA g^{-1} for activation and then at 520 mA g^{-1} in the subsequent cycles. (d) Rate performance of the P−CNT hybrid/c-NaCMC−CA electrode. All of the capacity was calculated based on the mass of phosphorus.

polymer binder, while the c-NaCMC−CA film remains undissolved after 2 days' storage in deionized water (Figure 4d). This further demonstrates the cross-linked nature of the c-NaCMC−CA system. The NaCMC has −OH groups that can chemically bond with carboxyl groups on CNTs, supported by the new carboxylate (O═C−O) stretching peak (1592 cm^{-1}) of ester groups.[11,48] This was further confirmed by the insoluble CNT−NaCMC film (Figure 4e) in deionized water. Strong interactions through chemical bonding of the binder to active material have been previously identified as one of the most critical factors affecting the stability of electrodes using high-volume-change materials.[2,11] In addition, 3D-cross-linked networks can also commonly endure large volume change with less structural degradation than conventional lineal polymer binders. This c-NaCMC−CA binder thus combines both advantages into one robust package.

The covalent bonds between phosphorus, CNTs, and the cross-linked polymer binder are expected to lead to a significant improvement in the electrochemical performance of the P−CNT anode over more conventional phosphorus anode designs. To test this, electrodes composed of P−CNT hybrid, carbon black, and c-NaCMC−CA binder (70:15:15, weight ratio) were used as working electrodes, and sodium was used as counter electrodes. To demonstrate the important role of the chemically bonded P−CNT composite structure, ball-milled phosphorus was hand-mixed with CNT and used as a control sample, denoted as a P/CNT mixture. In addition, the P−CNT hybrid anodes with just NaCMC binder were also prepared following the same protocol and compared with the cells with c-NaCMC−CA binder. The cells were tested at a current density of 260 mA g^{-1} at the first cycle for activation and then switched to a higher current density of 520 mA g^{-1} in the subsequent cycles. All of the capacity was calculated on the basis of the mass of phosphorus in this study considering the negligible capacity contribution of CNT in sodium ion batteries (~30 mAh/g, Figure S2). The typical initial charge/discharge voltage profiles of these three samples in the voltage range of 0.01−2 V are shown in Figure 5a. The P−CNT hybrid anodes with both NaCMC and c-NaCMC−CA binder show similar voltage profiles: Two plateaus at around 0.60 and 0.25 V in the sodiation process and three plateaus at around 0.5 V, 0.7 and 1.4 V in the reverse desodiation process were observed, which resemble the CV results in Figure S3 and are also consistent with the literature.[33] Noticeably, the P/CNT mixture anode has a large polarization compared with the P−CNT hybrid anodes and exhibits a relatively low specific capacity with a large irreversible capacity loss in the first cycle. This is also reflected by the very weak anodic peak in the CV

curve of the P−CNT mixture anode in Figure S3. The P−CNT hybrid anode delivers an initial capacity of ~2100 mAh g^{-1} (corresponding to ~81% of the theoretical capacity) with high initial Coulombic efficiency (ICE) (>81%) with both NaCMC and c-NaCMC−CA binder (Figure 5b,c). Both the capacity and ICE for the hybrid anode with cross-linked polymer binder are higher than that with NaCMC binder (2134.7 mAh g^{-1} *vs* 2113.3 mAh g^{-1}, 84.7% *vs* 81.7%). More importantly, the P−CNT hybrid anode with c-NaCMC−CA binder still had a high capacity of 1586.2 mAh g^{-1} after 100 cycles, which is ~91.7% capacity retention relative to the second-cycle capacity of 1729.4 mAh g^{-1}. Although the P−CNT hybrid anode with NaCMC binder shows a faster capacity fading (~1046 mAh g^{-1} after 100 cycles), it still shows much better cycling life when compared to the P/CNT mixture control sample (only 81 mAh g^{-1} after 100 cycles). To the best of our knowledge, this is the first report of a phosphorus-based anode with such a high reversible capacity (>1500 mAh g^{-1}) and capacity retention (>90%) after 100 cycles.

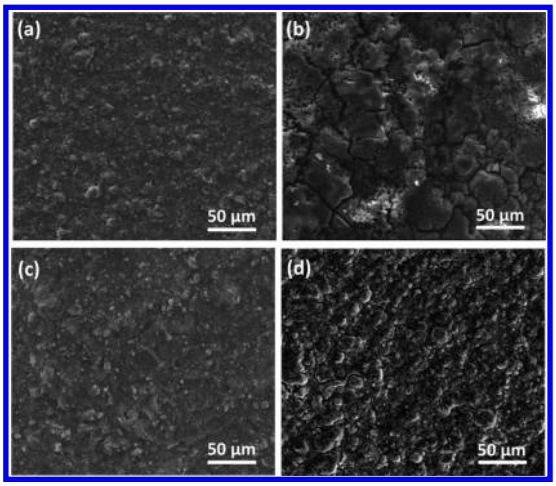

Figure 6. SEM images of the P−CNT hybrid anode with NaCMC binder (a) before and (b) after 60 cycles. SEM images of the P−CNT hybrid anode with c-NaCMC−CA cross-linked polymer binder (c) before and (d) after 60 cycles.

We also evaluated the rate performance of the anode using the P−CNT hybrid and c-NaCMC−CA binder with current densities ranging from 200 to 5.2 A g^{-1}, as shown in Figure 5d. As the current density increased, a specific capacity of 2245, ~1770, ~1570, and ~1340 mAh g^{-1} was obtained at 200, 520, 1.3, and 2.6 A g^{-1}, respectively. Even at 5.2 A g^{-1}, the hybrid anode still can deliver a high reversible capacity of ~850 mAh g^{-1}. When the rate was restored to 520 mA g^{-1} after 40 cycles of rate testing, the specific capacity of the P−CNT hybrid anode returned to 1250 mAh g^{-1}, close to the 1270 mAh g^{-1} from the initial 520 mA g^{-1} trial. This indicates that the anode charge/discharge was reversible even at high current density.

To better understand the effect of multiple chemical bonding among electrode components, electrochemical impedance spectroscopy (EIS) and SEM characterizations were performed. The Nyquist plots of these electrodes in Figure S4 consist of a single depressed semicircle in the high-medium frequency region and an inclined line at the low frequency. The EIS spectra at 20th cycle and 50th curves is almost overlapped for P−CNT hybrid/c-NaCMC−CA anode; slightly and much increased semicircle diameter were observed for the P−CNT hybrid/NaCMC electrode and P−CNT mixture/NaCMC electrode, respectively. According to

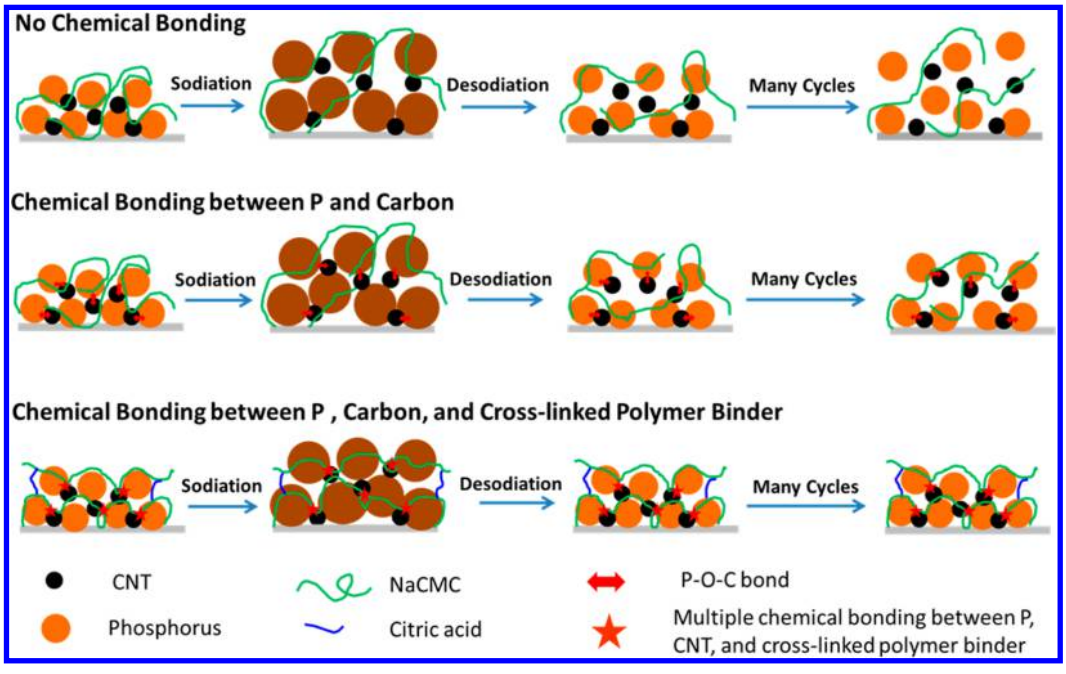

Figure 7. Schematic illustration of structure evolution of the phosphorus-base anode during cycling.

the literature and our previous study, the semicircle in EIS spectra relates to the impedance of sodium-ion transport through surface films and charge transfer at the electrode/electrolyte interface.[37,38] Obviously, without the chemical bonding between these electrode components, the impedance increase a lot during the cycle, suggesting an increased resistance for charge transfer at the electrode/electrolyte interface and Na^+ transport through the surface films (SEI) for the P−CNT mixture/NaCMC sample. The relatively stable SEI and lower resistance of P−CNT hybrid/c-NaCMC−CA electrode is believed due to chemical-bonding-induced synergetic effects. The P−O−C bonding in the P−CNT hybrid enables intimate electrical contact of phosphorus and CNT, and thus tolerance for successive volume change of phosphorus upon cycling. This leads to fast electron transfer and better cycling stability, which was reflected by lower polarization of the cell in Figure 5a and good rate performance in Figure 5d. SEM images of the post-cycling electrode in Figure 6 show large cracks in electrodes with NaCMC binder, while the relatively continuous morphology was observed by using c-NaCMC−CA binder, suggesting well maintenance of the electrode structure. As illustrated in Figure 7, the better structure stability at electrode level is attributed to the 3D-cross-linked network of the c-NaCMC−CA polymer and its chemical bonding with functional CNTs, helping maintain the structure of the electrode as a whole.

CONCLUSION

In summary, we have demonstrated a high-capacity, long-cycle-life phosphorus−CNT-cross-linked polymer binder composite anode for sodium ion battery based on a chemically bonded P−CNT hybrid and cross-linked polymer binder through a multiple bonding strategy. The P−O−C bond formed in the mechanical synthesis endows intimate contact of phosphorus and CNT. This electrode material was further integrated *via* chemical bonding with an efficient cross-linked polymer network to form robust electrodes. As a result, a high reversible capacity of 2134 mAh g^{-1} and good cycling stability (~91% capacity retention relative to the second-cycle capacity after 100 cycles) were achieved, which are outstanding results for the P-based sodium ion anode. The robust electrode constructed *via* the multicomponent chemical bonding strategy here may also be applicable to other high-performance conversion electrode materials with long cycle life.

EXPERIMENTAL SECTION

Preparation of P−CNT Hybrid. The P−CNT hybrid was synthesized through a simple ball-milling approach. The mixture of commercial phosphorus (Afla Aesar, 99%) and multiwalled carbon nanotubes functionalized with carboxylic acid groups (1.55 wt % −COOH content, Chengdu Organic Chemicals Co., China) with a mass ratio of 7:3 was placed in a stainless steel jar and sealed in a glovebox under argon protection, followed by ball-milling for 1 day at a speed of 400 rpm.

Characterization. Powder X-ray diffraction (XRD) was collected on a Rigaku Miniflex II spectrometer with Cu Kα radiation. The morphology of the P−CNT hybrid was investigated via scanning electron microscopy (Nano630 FE-SEM). Energy-filtered transmission electron microscopy (EF-TEM, JEOL 2010 LaB_6) was used for the microstructure investigation and elemental mapping. Fourier transform infrared spectrometry (FTIR) was performed on a Bruker Vertex V70 spectrometer in diffuse reflection mode with a Spectra Tech Collector II accessory. X-ray photoelectron spectroscopy (XPS) measurements were carried out with a Kratos XSAM800 Ultra spectrometer.

Electrochemical Measurements. Electrochemical tests were performed by using 2016 coin-type half cells assembled with sodium metal as the counter electrode in an argon-filled glovebox. The composites were prepared by coating slurries containing P−CNT active materials (70 wt %), Super P acetylene black (15 wt %), and polymer binder (15 wt %) on copper foil. The typical active material loading of the electrodes was 0.8−1 mg/cm^2. To well integrate all the electrode components, we developed a novel cross-linked polymer binder of sodium carboxymethylcellulose−citric acid (NaCMC−CA, 9:1, wt/wt), in which citric acid functioned as a cross-linker to form 3D network when drying the electrode at 150 °C for 2 h. The pure sodium carboxymethyl cellulose binder in the absence of citric acid cross-linker was also studied for the purpose of comparison. Moreover, to demonstrate the important role of the chemical bonding between P and CNT, the P/CNT mixture control sample without any chemical bonding was also prepared as follows: ball-milled phosphorus was simply hand-milled with CNT with the mass ratio of 7:3 and used as the active material for the control cells by following the above cell fabrication protocol.

The electrolyte consists of 1 mol/L $NaClO_4$ in a mixture of ethylene carbonate and diethyl carbonate (1:1 by volume) and fluoroethylene carbonate (FEC, 10 vol %). Galvanostatic charge/discharge tests were carried out on a LANDHE battery tester between 0.01 and 2.0 V *versus* Na/Na^+. Cyclic voltammetry (CV) was performed at a scan rate of 0.1 mV/s within the range of 0−2.5 V using a CHI 660D electrochemical workstation. Electrochemical impedance spectroscopy (EIS) was carried out by applying a perturbation voltage of 5 mV between 1 Hz and 10^5 Hz using a Solatron SI 1260 impedance analyzer.

Conflict of Interest: The authors declare no competing financial interest.

Acknowledgment. We acknowledge financial support from the U.S. Department of Energy's (DOE's) Office of Electricity Delivery & Energy Reliability (OE) (under Contract No. 57558). We also are grateful for enlightening discussions with Dr. Imre Gyuk of the DOE-OE Grid Storage Program. H.P. and D.W. acknowledge financial support from a Visiting Scholarship Fund from the State Key Laboratory of Molecular Engineering of Polymers at Fudan University.

Supporting Information Available: The Supporting Information is available free of charge on the ACS Publications website at DOI: 10.1021/acsnano.5b04474.

Selected area electron diffraction pattern of the P−CNT hybrid, cyclic voltammetry scanning of the P−CNT hybrid anode with c-NaCMC−CA binder, and Nyquist plots of the P−CNT hybrid/c-NaCMC−CA anode before and after cycling (PDF)

REFERENCES AND NOTES

1. Armand, M.; Tarascon, J. M. Building Better Batteries. *Nature* **2008**, *451*, 652–657.

2. Kovalenko, I.; Zdyrko, B.; Magasinski, A.; Hertzberg, B.; Milicev, Z.; Burtovyy, R.; Luzinov, I.; Yushin, G. A Major Constituent of Brown Algae for Use in High-Capacity Li-Ion Batteries. *Science* **2011**, *334*, 75–79.
3. Wu, F.; Lee, J. T.; Nitta, N.; Kim, H.; Borodin, O.; Yushin, G. Lithium Iodide as a Promising Electrolyte Additive for Lithium–Sulfur Batteries: Mechanisms of Performance Enhancement. *Adv. Mater.* **2015**, *27*, 101–108.
4. Wu, H.; Cui, Y. Designing Nanostructured Si Anodes for High Energy Lithium Ion Batteries. *Nano Today* **2012**, *7*, 414–429.
5. Manthiram, A.; Fu, Y.; Chung, S.-H.; Zu, C.; Su, Y.-S. Rechargeable Lithium–Sulfur Batteries. *Chem. Rev.* **2014**, *114*, 11751–11787.
6. Liang, J.; Yu, X.-Y.; Zhou, H.; Wu, H. B.; Ding, S.; Lou, X. W. Bowl-Like SnO_2@Carbon Hollow Particles as an Advanced Anode Material for Lithium-Ion Batteries. *Angew. Chem., Int. Ed.* **2014**, *53*, 12803–12807.
7. Ji, X.; Lee, K. T.; Nazar, L. F. A Highly Ordered Nanostructured Carbon-Sulphur Cathode for Lithium-Sulphur Batteries. *Nat. Mater.* **2009**, *8*, 500–506.
8. Bogart, T. D.; Oka, D.; Lu, X.; Gu, M.; Wang, C.; Korgel, B. A. Lithium Ion Battery Peformance of Silicon Nanowires with Carbon Skin. *ACS Nano* **2014**, *8*, 915–922.
9. Zhong, Y.; Yang, M.; Zhou, X.; Luo, Y.; Wei, J.; Zhou, Z. Orderly Packed Anodes for High-Power Lithium-Ion Batteries with Super-Long Cycle Life: Rational Design of $MnCO_3$/Large-Area Graphene Composites. *Adv. Mater.* **2015**, *27*, 806–812.
10. Zhou, W.; Chen, H.; Yu, Y.; Wang, D.; Cui, Z.; DiSalvo, F. J.; Abruña, H. D. Amylopectin Wrapped Graphene Oxide/Sulfur for Improved Cyclability of Lithium–Sulfur Battery. *ACS Nano* **2013**, *7*, 8801–8808.
11. Song, J.; Zhou, M.; Yi, R.; Xu, T.; Gordin, M. L.; Tang, D.; Yu, Z.; Regula, M.; Wang, D. Interpenetrated Gel Polymer Binder for High-Performance Silicon Anodes in Lithium-Ion Batteries. *Adv. Funct. Mater.* **2014**, *24*, 5904–5910.
12. Chan, C. K.; Peng, H.; Liu, G.; McIlwrath, K.; Zhang, X. F.; Huggins, R. A.; Cui, Y. High-Performance Lithium Battery Anodes Using Silicon Nanowires. *Nat. Nanotechnol.* **2008**, *3*, 31–35.
13. Zhou, M.; Gordin, M. L.; Chen, S.; Xu, T.; Song, J.; Lv, D.; Wang, D. Enhanced Performance of SiO/Fe_2O_3 Composite as an Anode for Rechargeable Li-Ion Batteries. *Electrochem. Commun.* **2013**, *28*, 79–82.
14. Yi, R.; Chen, S.; Song, J.; Gordin, M. L.; Manivannan, A.; Wang, D. High-Performance Hybrid Supercapacitor Enabled by a High-Rate Si-Based Anode. *Adv. Funct. Mater.* **2014**, *24*, 7433–7439.
15. Yabuuchi, N.; Kubota, K.; Dahbi, M.; Komaba, S. Research Development on Sodium-Ion Batteries. *Chem. Rev.* **2014**, *114*, 11636–11682.
16. Dunn, B.; Kamath, H.; Tarascon, J.-M. Electrical Energy Storage for the Grid: A Battery of Choices. *Science* **2011**, *334*, 928–935.
17. Ma, X.; Ning, G.; Qi, C.; Xu, C.; Gao, J. Phosphorus and Nitrogen Dual-Doped Few-Layered Porous Graphene: A High-Performance Anode Material for Lithium-Ion Batteries. *ACS Appl. Mater. Interfaces* **2014**, *6*, 14415–14422.
18. Xu, J.; Wang, M.; Wickramaratne, N. P.; Jaroniec, M.; Dou, S.; Dai, L. High-Performance Sodium Ion Batteries Based on Three-Dimensional Anode from Nitrogen-Doped Graphene Foams. *Adv. Mater.* **2015**, *27*, 2042.
19. Zhu, Y.; Han, X.; Xu, Y.; Liu, Y.; Zheng, S.; Xu, K.; Hu, L.; Wang, C. Electrospun Sb/C Fibers for a Stable and Fast Sodium-Ion Battery Anode. *ACS Nano* **2013**, *7*, 6378–6386.
20. Magasinski, A.; Zdyrko, B.; Kovalenko, I.; Hertzberg, B.; Burtovyy, R.; Huebner, C. F.; Fuller, T. F.; Luzinov, I.; Yushin, G. Toward Efficient Binders for Li-Ion Battery Si-Based Anodes: Polyacrylic Acid. *ACS Appl. Mater. Interfaces* **2010**, *2*, 3004–3010.
21. Slater, M. D.; Kim, D.; Lee, E.; Johnson, C. S. Sodium-Ion Batteries. *Adv. Funct. Mater.* **2013**, *23*, 947–958.
22. Palomares, V.; Serras, P.; Villaluenga, I.; Hueso, K. B.; Carretero-Gonzalez, J.; Rojo, T. Na-Ion Batteries, Recent Advances and Present Challenges to Become Low Cost Energy Storage Systems. *Energy Environ. Sci.* **2012**, *5*, 5884–5901.
23. Kim, Y.; Kim, Y.; Choi, A.; Woo, S.; Mok, D.; Choi, N.-S.; Jung, Y. S.; Ryu, J. H.; Oh, S. M.; Lee, K. T. Tin Phosphide as a Promising Anode Material for Na-Ion Batteries. *Adv. Mater.* **2014**, *26*, 4139–4144.
24. Li, W.; Chou, S.-L.; Wang, J.-Z.; Kim, J. H.; Liu, H.-K.; Dou, S.-X. $Sn_{4+x}P_3$ @ Amorphous Sn-P Composites as Anodes for Sodium-Ion Batteries with Low Cost, High Capacity, Long Life, and Superior Rate Capability. *Adv. Mater.* **2014**, *26*, 4037–4042.
25. Qian, J.; Xiong, Y.; Cao, Y.; Ai, X.; Yang, H. Synergistic Na-Storage Reactions in Sn_4P_3 as a High-Capacity, Cycle-Stable Anode of Na-Ion Batteries. *Nano Lett.* **2014**, *14*, 1865–1869.
26. Jache, B.; Adelhelm, P. Use of Graphite as a Highly Reversible Electrode with Superior Cycle Life for Sodium-Ion Batteries by Making Use of Co-Intercalation Phenomena. *Angew. Chem., Int. Ed.* **2014**, *53*, 10169–73.
27. Wen, Y.; He, K.; Zhu, Y.; Han, F.; Xu, Y.; Matsuda, I.; Ishii, Y.; Cumings, J.; Wang, C. Expanded Graphite as Superior Anode for Sodium-Ion Batteries. *Nat. Commun.* **2014**, *5*, 4033.
28. Su, D.; Dou, S.; Wang, G. Ultrathin MoS_2 Nanosheets as Anode Materials for Sodium-Ion Batteries with Superior Performance. *Adv. Energy Mater.* **2015**, *5*, 1401205.
29. Tang, K.; Fu, L.; White, R. J.; Yu, L.; Titirici, M.-M.; Antonietti, M.; Maier, J. Hollow Carbon Nanospheres with Superior Rate Capability for Sodium-Based Batteries. *Adv. Energy Mater.* **2012**, *2*, 873–877.
30. Lacey, S. D.; Wan, J.; Cresce, A. v. W.; Russell, S. M.; Dai, J.; Bao, W.; Xu, K.; Hu, L. Atomic Force Microscopy Studies on Molybdenum Disulfide Flakes as Sodium-Ion Anodes. *Nano Lett.* **2015**, *15*, 1018–1024.
31. Kim, S.-W.; Seo, D.-H.; Ma, X.; Ceder, G.; Kang, K. Electrode Materials for Rechargeable Sodium-Ion Batteries: Potential Alternatives to Current Lithium-Ion Batteries. *Adv. Energy Mater.* **2012**, *2*, 710–721.
32. Li, W. J.; Chou, S. L.; Wang, J. Z.; Liu, H. K.; Dou, S. X. Simply Mixed Commercial Red Phosphorus and Carbon Nanotube Composite with Exceptionally Reversible Sodium-Ion Storage. *Nano Lett.* **2013**, *13*, 5480–5484.
33. Qian, J.; Wu, X.; Cao, Y.; Ai, X.; Yang, H. High Capacity and Rate Capability of Amorphous Phosphorus for Sodium Ion Batteries. *Angew. Chem., Int. Ed.* **2013**, *52*, 4633–4636.
34. Kim, Y.; Park, Y.; Choi, A.; Choi, N. S.; Kim, J.; Lee, J.; Ryu, J. H.; Oh, S. M.; Lee, K. T. An Amorphous Red Phosphorus/Carbon Composite as a Promising Anode Material for Sodium Ion Batteries. *Adv. Mater.* **2013**, *25*, 3045–3049.
35. Yabuuchi, N.; Matsuura, Y.; Ishikawa, T.; Kuze, S.; Son, J.-Y.; Cui, Y.-T.; Oji, H.; Komaba, S. Phosphorus Electrodes in Sodium Cells: Small Volume Expansion by Sodiation and the Surface-Stabilization Mechanism in Aprotic Solvent. *ChemElectroChem* **2014**, *1*, 580–589.
36. Zhu, Y.; Wen, Y.; Fan, X.; Gao, T.; Han, F.; Luo, C.; Liou, S.-C.; Wang, C. Red Phosphorus–Single-Walled Carbon Nanotube Composite as a Superior Anode for Sodium Ion Batteries. *ACS Nano* **2015**, *9*, 3254–3264.
37. Sun, J.; Zheng, G.; Lee, H.-W.; Liu, N.; Wang, H.; Yao, H.; Yang, W.; Cui, Y. Formation of Stable Phosphorus–Carbon Bond for Enhanced Performance in Black Phosphorus Nanoparticle–Graphite Composite Battery Anodes. *Nano Lett.* **2014**, *14*, 4573–4580.
38. Song, J.; Yu, Z.; Gordin, M. L.; Hu, S.; Yi, R.; Tang, D.; Walter, T.; Regula, M.; Choi, D.; Li, X.; Manivannan, A.; Wang, D. Chemically Bonded Phosphorus/Graphene Hybrid as a High Performance Anode for Sodium-Ion Batteries. *Nano Lett.* **2014**, *14*, 6329–6335.
39. Fu, Y.; Zhang, L.; Chen, G. Preparation of a Carbon Nanotube-Copper Nanoparticle Hybrid by Chemical Reduction for Use in the Electrochemical Sensing of Carbohydrates. *Carbon* **2012**, *50*, 2563–2570.
40. Song, J.; Chen, S.; Zhou, M.; Xu, T.; Lv, D.; Gordin, M. L.; Long, T.; Melnyk, M.; Wang, D. Micro-Sized Silicon-Carbon

Composites Composed of Carbon-Coated Sub-10 nm Si Primary Particles as High-Performance Anode Materials for Lithium-Ion Batteries. *J. Mater. Chem. A* **2014**, *2*, 1257–1262.
41. Daasch, L.; Smith, D. Infrared Spectra of Phosphorus Compounds. *Anal. Chem.* **1951**, *23*, 853–868.
42. Perez-Romo, P.; Potvin, C.; Manoli, J. M.; Chehimi, M. M.; Djéga-Mariadassou, G. Phosphorus-Doped Molybdenum Oxynitrides and Oxygen-Modified Molybdenum Carbides: Synthesis, Characterization, and Determination of Turnover Rates for Propene Hydrogenation. *J. Catal.* **2002**, *208*, 187–196.
43. Puziy, A. M.; Poddubnaya, O. I.; Socha, R. P.; Gurgul, J.; Wisniewski, M. XPS and NMR Studies of Phosphoric Acid Activated Carbons. *Carbon* **2008**, *46*, 2113–2123.
44. Zheng, Z.; Liu, S.; Cui, X.; Wang, H.; Wang, B.; Yang, T. Preparation of a Novel Phosphorus- and Nitrogen-Containing Flame Retardant and Its Synergistic Effect in the Intumescent Flame-Retarding Polypropylene System. *Polym. Compos.* **2015**, *36*, 1606–1619.
45. Park, S.-J.; Zhao, H.; Ai, G.; Wang, C.; Song, X.; Yuca, N.; Battaglia, V. S.; Yang, W.; Liu, G. Side-Chain Conducting and Phase-Separated Polymeric Binders for High-Performance Silicon Anodes in Lithium-Ion Batteries. *J. Am. Chem. Soc.* **2015**, *137*, 2565.
46. Gorgieva, S.; Kokol, V. Synthesis and Application of New Temperature-Responsive Hydrogels Based on Carboxymethyl and Hydroxyethyl Cellulose Derivatives for the Functional Finishing of Cotton Knitwear. *Carbohydr. Polym.* **2011**, *85*, 664–673.
47. Demitri, C.; Del Sole, R.; Scalera, F.; Sannino, A.; Vasapollo, G.; Maffezzoli, A.; Ambrosio, L.; Nicolais, L. Novel Superabsorbent Cellulose-Based Hydrogels Crosslinked with Citric Acid. *J. Appl. Polym. Sci.* **2008**, *110*, 2453–2460.
48. Koo, B.; Kim, H.; Cho, Y.; Lee, K. T.; Choi, N.-S.; Cho, J. A Highly Cross-Linked Polymeric Binder for High-Performance Silicon Negative Electrodes in Lithium Ion Batteries. *Angew. Chem., Int. Ed.* **2012**, *51*, 8762–8767.